Chitosan-Decorated Doxorubicin-Encapsulated Nanoparticle Targets and Eliminates Tumor Reinitiating Cancer Stem-like Cells

Wei Rao,[†,‡,¶] Hai Wang,[†,‡,§,¶] Jianfeng Han,[§,∥] Shuting Zhao,[†,‡] Jenna Dumbleton,[†,‡] Pranay Agarwal,[†,‡] Wujie Zhang,[⊥] Gang Zhao,[#] Jianhua Yu,[§,∥] Debra L. Zynger,[▽] Xiongbin Lu,[○] and Xiaoming He*[,†,‡,§]

[†]Department of Biomedical Engineering, The Ohio State University, Columbus, Ohio 43210, United States, [‡]Davis Heart and Lung Research Institute, The Ohio State University, Columbus, Ohio 43210, United States, [§]Comprehensive Cancer Center, The Ohio State University, Columbus, Ohio 43210, United States, [∥]Division of Hematology, The Ohio State University, Columbus, Ohio 43210, United States, [⊥]Biomolecular Engineering Program, Department of Physics and Chemistry, Milwaukee School of Engineering, Milwaukee, Wisconsin 53202, United States, [#]Centre for Biomedical Engineering, Department of Electronic Science and Technology, University of Science and Technology of China, Hefei, Anhui 230027, China, [▽]Division of Genitourinary Pathology, The Ohio State University, Columbus, Ohio 43210, United States, and [○]Department of Cancer Biology, The University of Texas MD Anderson Cancer Center, Houston, Texas 77030, United States. [¶]These authors contributed equally.

ABSTRACT Tumor reinitiating cancer stem-like cells are responsible for cancer recurrence associated with conventional chemotherapy. We developed a doxorubicin-encapsulated polymeric nanoparticle surface-decorated with chitosan that can specifically target the CD44 receptors of these cells. This nanoparticle system was engineered to release the doxorubicin in acidic environments, which occurs when the nanoparticles are localized in the acidic tumor microenvironment and when they are internalized and localized in the cellular endosomes/lysosomes. This nanoparticle design strategy increases the cytotoxicity of the doxorubicin by six times in comparison to the use of free doxorubicin for eliminating $CD44^+$ cancer stem-like cells residing in 3D mammary tumor spheroids (*i.e.*, mammospheres). We further show these nanoparticles reduced the size of tumors in an orthotopic xenograft tumor model with no evident systemic toxicity. The development of nanoparticle system to target cancer stem-like cells with low systemic toxicity provides a new treatment arsenal for improving the survival of cancer patients.

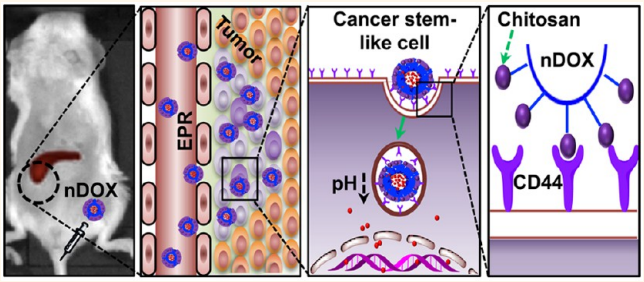

KEYWORDS: chitosan · CD44 · targeting · EPR · cancer stem-like cell · nanoparticle

Cancer stem-like cells (CSLCs) are rare cell populations in a tumor that overexpress CD44 receptors. Many therapeutic agents can shrink the size of a tumor, but if they do not kill these cells, a tumor can regrow because these cells are capable of differentiating and producing cells that can reinitiate and maintain tumor growth.[1−5] Unlike conventional tumor cells, many anticancer drugs cannot kill these cells.[1−9] For example, the treatment of breast cancer with free doxorubicin hydrochloride (DOX) was unable to effectively eradicate CSLCs. The reason for this is that CSLCs have high drug resistance.[10−12]

To overcome drug resistance of non-stem cancer cells, tremendous effort has been made to develop organic and inorganic nanoscale drug delivery systems. It has been shown that DOX tethered on gold or entrapped in either silica or polymeric nanoparticles can facilitate its intracellular delivery to overcome drug resistance of non-stem cancer cells in 2D cell cultures,[13−15] where the drug resistance is a result of overexpression of transmembrane P-glycoprotein transporters that utilize energy from ATP hydrolysis to pump out free anticancer drugs. However, the drug resistance of CSLCs are much more complex. Besides the overexpression of transmembrane ABC

* Address correspondence to he.429@osu.edu.

Received for review December 4, 2014 and accepted May 25, 2015.

Published online May 25, 2015
10.1021/nn506928p

(ATP-binding cassette) transporters that pump out free anticancer drugs, the drug resistance of CSLCs has been reported to be multifaceted due to both the intrinsic properties (*e.g.*, quiescence/dormancy and high resistance to apoptosis) and the extrinsic factors in their microenvironment or niche.[16−21]

Several recent studies show polymeric micelles or nanoparticles can enhance the accumulation of anticancer drug in 3D breast, glioblastoma, and gastric spheroids enriched with CSLCs.[22−26] Furthermore, CSLCs also overexpress CD44, which suggests that hyaluronic acid can be used to target these cells. These results suggest that the use nanoparticles and the coating with hyaluronic acid can selectively target and deliver drugs specifically to CSLCs.

Here, we developed a nanodrug (nanodoxorubicin or nDOX) system by encapsulating DOX in nanoparticles synthesized using Pluronic F127 cross-linked and surface-decorated with chitosan (Scheme 1a). Pluronic F127 is an amphiphilic copolymer consisting of hydrophilic polyethylene glycol (PEG) and the more hydrophobic polypropylene glycol (PPG).[27,28] Chitosan is a biocompatible and biodegradable natural polysaccharide derived from chitin, the second most abundant polysaccharide on earth after cellulose. Chitosan is increasingly used for various biomedical applications including drug and gene delivery, tissue engineering, wound healing, and antimicrobial.[29−32] The chemical structure of chitosan partially resembles that of HA, but it is positively charged. The positive charge may make these nanoparticles bind more efficiently to mammalian cells. We hypothesize the chitosan is capable of targeting the CD44 receptors commonly overexpressed on CSLCs but not the CD44 receptors expressed on normal stem cells (Scheme 1b). In addition, these nanoparticles are designed to degrade or expand in the acidic microenvironment in a tumor (pH ∼6) and in late endosomes and lysosomes (pH ∼4−5) (Scheme 1b).[33,34] After intravenous injection, the ∼20 nm nanoparticles will be transported into the tumor *via* the enhanced permeability and retention (EPR) effect[35−39] to actively target and internalize in $CD44^+$ CSLCs. The encapsulated drug will release out of the nanoparticle, diffuse into the cytosol, and eventually accumulate in the nuclei to produce cytotoxicity to CSLCs.

We will test the aforementioned hypothesis and strategy for targeting CLSCs but not normal stem cells with chitosan-decorated DOX-encapsulated nanoparticles *in vitro* using 3D-cultured mammary tumor spheroids (*i.e.*, mammospheres) enriched with CSLCs and spheroids of normal human adipose-derived stem cells. Moreover, we will examine the biodistribution, safety, and efficacy of the chitosan-decorated DOX-encapsulated nanoparticles for cancer treatment *in vivo* using an orthotopic xenograft human breast cancer model produced by injecting the mammosphere cells enriched with CSLCs into the mammary fat pad of immunodeficient mice.

RESULTS AND DISCUSSION

Characterization of Mammospheres Enriched with Human CSLCs. The 3D mammospheres enriched with human mammary CSLCs were prepared by culturing MCF-7 human breast cancer cells in ultralow attachment plates similar to that previously reported[45,46] with slight modifications as detailed in the Materials and Methods section. Typical electron microscopy images demonstrating no apparent change in the morphology of the resultant mammospheres at three different passages during *in vitro* culture with serial passaging are shown in Figure 1a. It is worth noting that the suspension culture in ultralow attachment plate in medium supplemented with various growth factors and chemicals promotes stemness (self-renewal) and suppresses the expression of estrogen receptor (ER).[40] The resultant mammospheres are not simple aggregates of regular or parent ER^+ MCF-7 cancer cells, but enriched with CSLCs with low or negligible ER expression.[41] The capability of self-renewal or stemness of the mammosphere cells is first evidenced by their capability of reinitiating a similar number of mammospheres (per 10 000 cells) during serial passaging *in vitro* (Figure 1b). This may explain why only 5000 mammosphere cells are required to produce orthotopic xenograft of human breast tumor in mice while the same number of regular ER^+ MCF-7 cancer cells could not.[26] To further examine the stemness of the mammosphere cells as compared to the parent MCF-7 cells (2D cultured by default), flow cytometry studies were performed first to study the expression of CD44, CD24, and CD133. These receptor markers have been widely used to identify CSLCs in various cancers.[9,42−44] Particularly, $CD44^+CD24^-$ cells were conventionally taken as mammary CSLCs with tumor initiating or reinitiating capability. Our data show that CD44 is highly overexpressed in nearly 50% of the mammospheres cells (Figure 1c). Furthermore, we noticed that the expression of CD24 in the 3D cultured mammosphere cells is extremely low (< ∼1%), but this receptor is highly expressed in the 2D cultured parent MCF-7 cells. As a result, the percentage of $CD44^+CD24^-$ cells is not much different from that of $CD44^+$ cells in mammosphere cells. Recent studies show that CD133 could be an important marker for breast CSLCs.[44] Therefore, we further investigated the characteristic of $CD44^+CD133^+$ subpopulation in the mammospheres. As shown in Supporting Information Figure S1a, compared to the 2D cultured parent MCF-7 cells, the $CD44^+CD133^+$ CSLCs were enriched by more than 15 times on average in the mammosphere cells.

To further examine the stemness of $CD44^+CD133^+$ mammosphere cells as compared to $CD44^+$ mammosphere cells, all mammosphere cells, and the parent

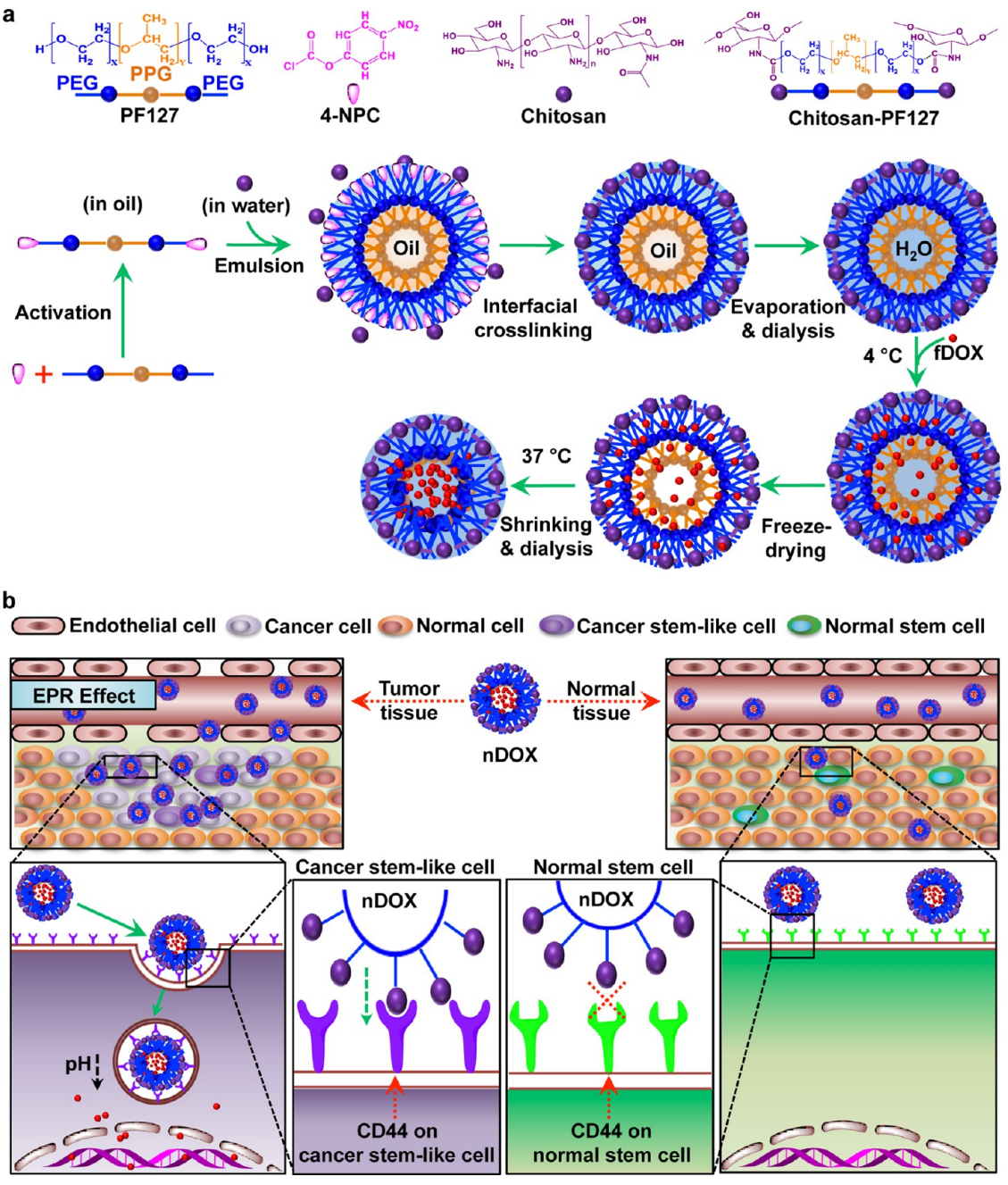

Scheme 1. A schematic illustration of the synthesis of nanoparticle-encapsulated doxorubicin hydrochloride (nDOX) and the anticancer mechanisms of nDOX. (a) The chemistry and procedure for producing the nDOX. To synthesize nanoparticles surface-decorated with chitosan, the PEG terminals of PF127 were partially activated with 4-NPC followed by oil-in-water emulsion and interfacial-cross-linking as a result of the reaction between 4-NPC (in oil) and chitosan (in water) on the oil−water interface. After removing organic solvent (*i.e.*, oil) by rotary evaporation and residual chemicals by dialysis, the nanoparticles were soaked with fDOX at 4 °C and then freeze-dried to remove water. To obtain clean nDOX, the samples were then shrunken at 37 °C in an incubator and further dialyzed at 37 °C to remove any fDOX outside the nanoparticles. (b) The capacity of the nDOX in targeting tumor *via* the EPR effect and the capability of the nDOX in binding (through chitosan decorated on its surface) to CD44 receptors overexpressed on cancer stem-like cells (CSLCs) but not normal stem cells together with pH dependent drug release from nDOX. PPG. polypropylene glycol; PEG. polyethylene glycol; PF127. Pluronic F127; 4-NPC. 4-nitrophenyl chloroformate; fDOX. free doxorubicin hydrochloride; EPR, enhanced permeability and retention (of tumor but not normal vasculature).

MCF-7 cells, quantitative RT-PCR studies were performed to understand the expression of three pluripotent stem cell genes (Oct4, Nanog, and Klf4) together with two epithelial lineage genes-cytokeratin 14 (CK14) for basal epithelium and CK18 for luminal epithelium.[45−47] As shown in Supporting Information Figure S1b, the expression of both Oct4 and Nanog in the mammosphere cells was significantly higher than that in the parent MCF-7 cells. The $CD44^+$ and $CD44^+CD133^+$ mammosphere cells have significantly

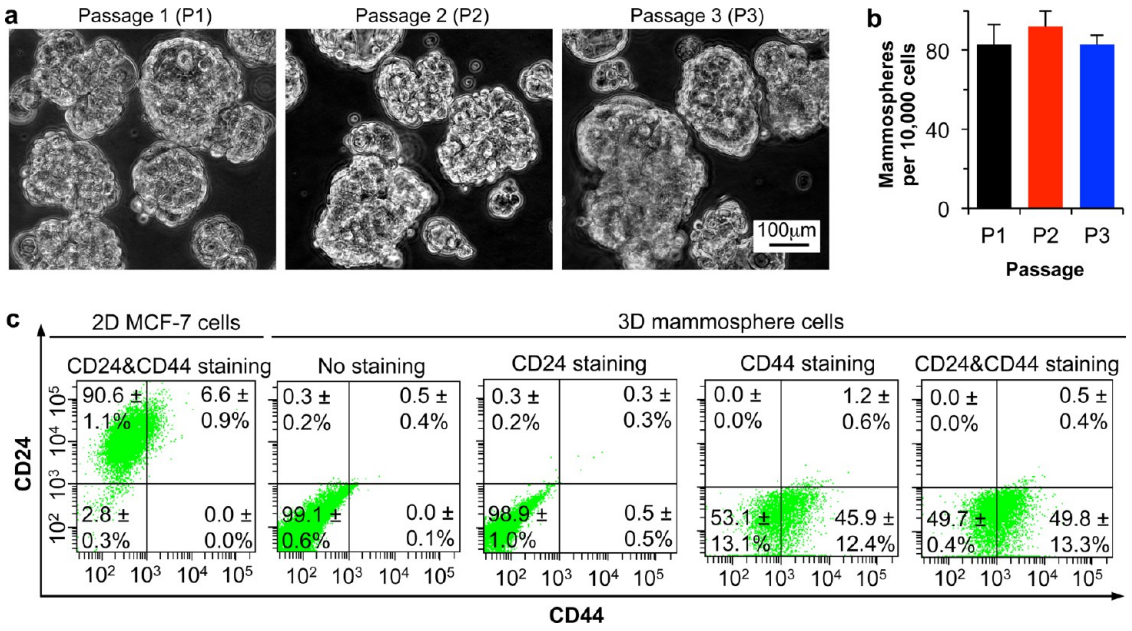

Figure 1. Characterization of 3D mammospheres enriched with mammary cancer stem-like cells (CSLCs) from MCF-7 human breast cancer cells showing their self-renewal capability *in vitro* and the expression of CD24 in mammosphere cells is negligible. (a) Typical micrographs of mammospheres at passages 1−3 showing no apparent change in morphology during *in vitro* culture by serial passaging under suspension culture in ultralow attachment plate. (b) Quantitative data showing no significant change in the efficiency of mammosphere formation at different passages. (c) Surface maker CD44 and CD24 staining of the mammosphere cells showing that ~99% mammosphere cells are $CD24^-$ and the percentage of $CD44^+CD24^-$ cell subpopulation of is not significantly different from that of $CD44^+$.

higher expression of both Oct4 and Nanog than all mammosphere cells. For Klf4, its expression in all mammosphere cells was similar to that in MCF-7 cells. More importantly, $CD44^+$ and $CD44^+CD133^+$ mammosphere cells have significantly (p = 0.01 and 0.0002, respectively) higher expression of Klf4 than all mammosphere cells. The Klf4 expression in $CD44^+CD133^+$ mammosphere cells is significantly (p = 0.02) higher than that in $CD44^+$ mammosphere cells.

By contrast, the CK18 gene, a marker for terminal differentiation into the luminal epithelial lineage,[45−47] was significantly more expressed in the MCF-7 cells than all mammosphere cells, $CD44^+$ mammosphere cells, and $CD44^+CD133^+$ mammosphere cells (with p = 0.0001, 0.000002, and 0.03, respectively). On the other hand, the expression of CK14 (a marker of early epithelial differentiation into the basal epithelial lineage[45−47]) was significantly higher in all mammosphere cells, $CD44^+$ mammosphere cells, and $CD44^+CD133^+$ mammosphere cells (p = 0.001, 4×10^{-9}, and 3×10^{-6}, respectively) than the parent MCF-7 cells. These data are consistent with the literature reporting that mammary CSLCs were probably originated from multipotent basal-like stem cells or luminal progenitor cells already committed to the epithelial lineages in the mammary gland.[45−47] Moreover, $CD44^+CD133^+$ mammosphere cells have significantly (p = 0.0001) higher CK14 expression than all mammosphere cells and $CD44^+$ mammosphere cells, while the CK14 expression is not different between all mammosphere cells and $CD44^+$ mammosphere cells. Taken together, the gene expression data shown in Supporting Information Figure S1b suggest that mammosphere cells have higher stemness than the parent MCF-7 cells and $CD44^+CD133^+$ mammosphere cells have the highest stemness, followed by $CD44^+$ mammosphere cells, and all mammosphere cells.

The observation that $CD44^+CD133^+$ mammosphere cells have the highest stemness compared to the other three cell populations is further supported by data from flow cytometry analyses of three stem cell protein markers: Oct4, Nanog, and Klf4. As shown in Supporting Information Figure S1c, mammosphere cells have significantly (p = 0.02) higher expression of Oct4 than MCF-7 cells, $CD44^+$ mammosphere cells have significantly (p = 0.003) higher expression of Oct4 than all mammosphere cells, and $CD44^+CD133^+$ mammosphere cells have significantly (p = 0.02) higher expression of Oct4 than $CD44^+$ mammosphere cells. The $CD44^+CD133^+$ mammosphere cells also have significantly higher expression of Nanog and Klf4 proteins than the other three cell populations. These data indicate $CD44^+CD133^+$ mammosphere cells have the highest pluripotency or stemness at the level of both gene and protein expression, which validates the use of CD133 in addition to CD44 and CD24 for judging the possible CSLCs in the mammosphere cells although more markers might be needed to more definitively identify the CSLCs.

Characterization of nDOX. We loaded our nanoparticles with the commercially available hydrophilic,

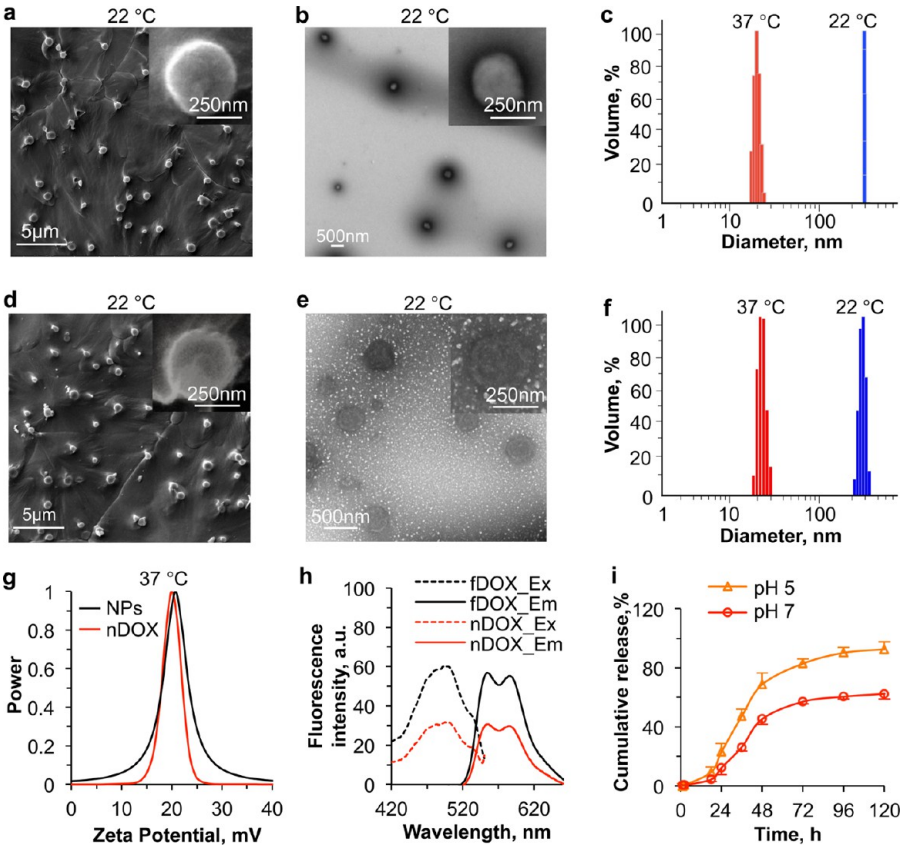

Figure 2. Characterization of Pluronic F127-chitosan nanoparticles (NPs) and doxorubicin (DOX) encapsulated in the nanoparticles (nDOX) showing their round morphology, thermal responsiveness in size (small at 37 °C), positively charged surface, intact fluorescent property, and (for nDOX only) pH dependent drug release. (a) A typical SEM image of NPs at 22 °C. (b) A typical TEM image of NPs at 22 °C. (c) Typical dynamic light scattering (DLS) data of NPs at 22 and 37 °C. (d) A typical SEM image of nDOX at 22 °C. (e) A typical TEM image of nDOX at 22 °C. (f) Typical dynamic light scattering (DLS) data of nDOX at 22 and 37 °C. (g) DLS zeta potential distribution of NPs and nDOX at 37 °C. (h) Excitation (Ex) and emission (Em) fluorescence spectra of nDOX and fDOX. (i) Release of encapsulated DOX from NPs at pH 5 and 7 at 37 °C.

water-soluble, and clinically used doxorubicin hydrochloride (DOX). We will refer to this nanoparticle-encapsulated DOX as nDox, while the free (*i.e.*, nonencapsulated) DOX will be referred to as fDox. These nanoparticles are made from Pluronic F127 and chitosan. The chemistry and procedure for synthesizing these nanoparticles were similar to those reported elsewhere[28] with slight modification as detailed in Materials and Methods and schematically illustrated in Scheme 1a. The total and cross-linked contents of chitosan in the nanoparticles was determined to be 8.3 ± 0.7% and 3.4 ± 0.6% in weight, respectively, using the peaks of Pluronic F127 and chitosan on the ^{1}H NMR spectrum of the nanoparticles (Supporting Information Figure S2). According to SEM (Figure 2a) and TEM (Figure 2b) images, the nanoparticles (empty with no drug) are round in shape with a core−shell structure (Figure 2b inset) and their size is ∼250−300 nm in diameter at 22 °C. This size is consistent with dynamic light scattering (DLS) measurement of the nanoparticles in DI water at the same temperature as shown in Figure 2c. The nanoparticles are much smaller (∼20 nm) at 37 °C. This thermally responsive property of the nanoparticles was utilized to encapsulate the hydrophilic fDOX by soaking them together in deionized (DI) water at 4 °C when the nanoparticles were bigger and highly permeable to allow for diffusion of fDOX into the nanoparticles (Scheme 1a). Following freeze-drying to remove water, the sample was heated to 37 °C to shrink the nanoparticles to a much smaller and compact size so that DOX could be effectively trapped in the nanoparticles. Next, the shrunken nanoparticle was dissolved in warm (37 °C) DI water in a dialysis bag and dialyzed against DI water at 37 °C to remove nonencapsulated fDOX. The sample was then either used immediately or dried at 37 °C for future use.

A typical SEM and TEM image of the dried nDOX at room temperature showing its round morphology is given in Figure 2, panels d and e, respectively. Although the SEM image of nDOX was similar to that of empty (*i.e.*, no drug) nanoparticles shown in Figure 2a, the core−shell morphology of the empty nanoparticles shown in Figure 2b was not as evident for nDOX. We speculate this is due to the encapsulation of DOX in the nanoparticle core. The DOX might be stained by uranium acetate in a similar manner to the polymeric shell and therefore, the contrast between

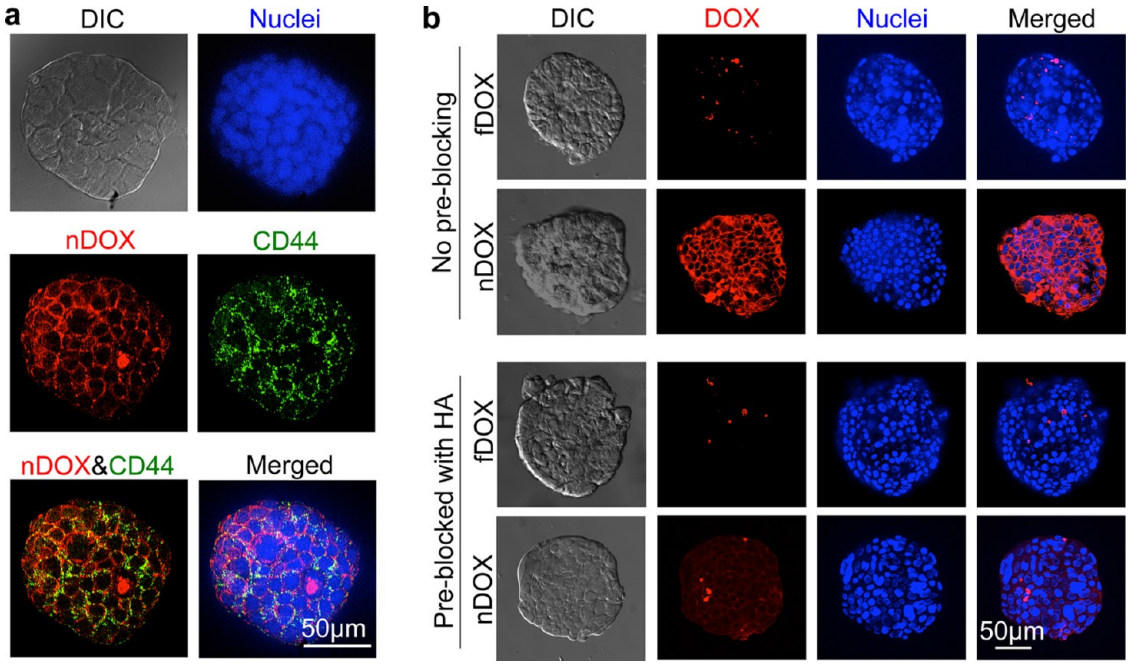

Figure 3. Zeiss ApoTome structured illumination microscopy (SIM, confocal-like) images of specific binding between nDOX and mammosphere cells at 4 °C (to minimize endocytosis for uptake) showing nDOX is capable of targeting CD44$^+$ mammosphere cells. (a) Co-localization of nDOX and CD44 receptors after incubation of nDOX and mammospheres at 4 °C for 3 h. (b) Preblocking the mammosphere cells with hyaluronic acid (HA), the natural ligand of CD44 receptors in the extracellular matrix of tumor, significantly reduces the binding between nDOX and the mammosphere cells. In all cases, binding between free DOX (fDOX) and mammosphere cells is negligible. DIC: differential interference contrast. The sample was excited at 558 nm to induce the fluorescence emission of fDOX and nDOX at 583 nm. For the green fluorescence of Alexa Fluor 488 at 525 nm to visualize CD44 receptor, the sample was excited at 490 nm. To visualize Hoechst stain of the cell nuclei, the sample was excited at 359 nm to emit blue fluorescence at 461 nm. The label of DOX in (b) refers to the fluorescence emission signal of both fDOX and nDOX.

the shell and the internal part of the nanoparticle is difficult to visualize by TEM. According to the image, the diameter of nDOX is ~250−300 nm at 22 °C, which was similar to that determined by DLS at the same temperature (271.9 ± 7.7 nm, Figure 2f). Moreover, the nDOX remains thermally responsive with a diameter of 21.4 ± 1.2 at 37 °C. The nDOX (as with empty nanoparticles) has a positively charged surface as indicated by its surface zeta potential of +21.3 ± 1.0 mV at 37 °C (Figure 2g), which together with its smaller size at 37 °C is important to facilitate cellular uptake of the nDOX. This is because living cells have a negatively charged plasma membrane with high electrostatic affinity to the positively charged nanoparticles and a diameter of ~20−30 nm may allow them to enter the tumor by the enhanced permeability and retention (EPR) effect. The encapsulation efficiency of DOX was 9.9 ± 0.9% in weight and the loading content was 1.98 ± 0.1 μg DOX/mg nanoparticles; both are within the range reported in the literature[33,51] for encapsulating hydrophilic drug using polymeric nanoparticles.[27,48] The fluorescence spectrum showed that nDOX has the same two fluorescence emission peaks at 555 and 585 nm as fDOX after excitation with a 490 nm laser (Figure 2h).

To confirm that the nDOX is pH responsive, we compared release of the encapsulated DOX from nanoparticles in 1 mL dialysis tube (MWCO: 20 kDa) into 30 mL of PBS at 37 °C at pH 7 and pH 5. As shown in Figure 2i, the release of nDOX was significantly faster at pH 5 than 7, suggesting that the acidic pH in tumor and in late endosomes and lysosomes should facilitate the release of DOX from the nanoparticles.

Assessing the Binding of nDOX to Cells Overexpressing CD44 Receptors. To show the capability of nDOX in targeting overexpressed CD44 receptors on the mammosphere cells including CSLCs (Figure 1c), we incubated the mammospheres with nDOX on ice (~4 °C), followed by fixing the mammospheres and then incubating the fixed mammospheres first with primary antibody of CD44 and then with secondary antibody tagged with a green fluorescent probe (Alexa Fluor 488) to visualize the CD44 receptors on the mammosphere cells. The incubation at ice temperature minimizes endocytosis and cellular uptake after binding to the CD44 receptor.[49] As shown in Figure 3a, nDOX could bind extensively on the mammosphere cells with negligible uptake by the cells when they were incubated at 4 °C. The yellowish appearance in the merged two-color (nDOX&CD44) image suggests the colocalization or close proximity between nDOX and CD44 receptors on the mammosphere cells.

We attribute this interaction between the nDOX and CD44 receptors on the mammosphere cells to

chitosan decorated on the nanoparticle surface. Hyaluronic acid (HA) is a natural ligand of CD44 receptors in the extracellular matrix of tumor.[26,50,51] Interestingly, HA and chitosan share a common chemical structural unit (*N*-acetyl-D-glucosamine) and this component may be responsible for the interaction with CD44 (see Supporting Information Figure S3). To confirm this hypothesis, we conducted further experiments to see how preblocking the $CD44^+$ mammosphere cells with HA could affect the binding of nDOX to the mammosphere cells by incubating the cells first with HA and then the nDOX at 4 °C. As shown in Figure 3b, preincubating the mammospheres with HA indeed minimized the binding between nDOX and the mammosphere cells, whereas binding between fDOX and mammosphere cells is negligible and not affected by preincubation with HA. The data shown in Figure 3 indicate that the nDOX could specifically bind to $CD44^+$ mammosphere cells, probably *via* the interactions between chitosan decorated on its surface and CD44 receptors on the mammosphere cells.

It is worth noting that although nDOX could bind to the CD44 receptors on the cancerous mammosphere cells including CSLCs, it does not necessarily bind to the CD44 receptors highly expressed on noncancerous stem cells. As shown in Supporting Information Figure S4, no apparent binding could be observed between our nDOX and the CD44 receptors overexpressed on the normal primary human adipose-derived stem cells (ADSCs) either cultured in 3D spheres (Supporting Information Figure S4a) or under 2D adherent culture (Supporting Information Figure S4b). These observations are probably due to the fact that CD44 has different isoforms[52] and the isoform of CD44 receptors on the cancerous mammosphere cells including CSLCs might be different from that on the normal stem cells. For example, mesenchymal stem cells have been shown to preferentially express standard CD44 isoform while variant isoforms with an enlarged size are expressed on malignant cancer cells.[4,5,53] Although it is still unclear how particular variations may affect the binding affinity of CD44 to its ligand, oligomers of some CD44 splice variants have increased affinity to HA (and possibly chitosan).[54] Although further investigations are needed to confirm this hypothesis, the observation that our nDOX could bind to CD44 on the human mammosphere cells but not the normal human ADSCs is exciting because it could further reduce the systemic toxicity of the nDOX *in vivo*. Lastly, it is interesting to note that according to Figure 3 and Supporting Information Figure S4, there was no observable fDOX in the mammosphere cells or ADSCs cultured in 3D spheroids after incubating the cells with the free drug at 4 °C for 3 h. It is clearly visible in the 2D cultured cells after the same treatment, suggesting the much higher capability of excluding free anticancer drug by the 3D than 2D cultured cells.

Comparing the Capability of nDOX with fDOX for Targeting CSLCs. To study the uptake of fDOX and nDOX by mammosphere cells, we incubated the drug with mammospheres at 37 °C (rather than 4 °C) for various times. Typical images showing the intracellular DOX together with the stains of nuclei and endo/lysosomes in cells incubated with fDOX and nDOX for 3 h are shown in Figure 4a. As expected, the red fluorescence of DOX was not observable in cells with no treatment (NT) or treated with empty nanoparticles (NPs) (Supporting Information Figure S5a). As shown in Figure 4a, fDOX taken up by the mammosphere cells after 3 h incubation at 37 °C was mostly located in cell nuclei and the intensity of fDOX fluorescence was weak, presumably due to resistance of the mammosphere cells including CSLCs to take up fDOX. By contrast, the red fluorescence was strong in the mammosphere cells incubated with nDOX. This observation presumably is a result of the binding (Figure 3) between chitosan on nDOX and CD44 receptors overexpressed in mammosphere cells to facilitate cellular uptake of the nDOX by endocytosis. The extensive overlap between the red fluorescence of nDOX and green stain of endo/lysosomes suggests that endocytosis mediated by the chitosan-CD44 interactions was the main mechanism for the uptake of nDOX by mammosphere cells. It is worth noting that the much higher uptake of nDOX by the mammosphere cells could also be because it could penetrate into the mammosphere better than fDOX possibly by receptor-mediated transcytosis.[39,50] However, this receptor mediated transcytosis should have little impact on the binding study shown in Figure 3 because little energy is available to drive receptor mediated transcytosis or endocytosis at 4 °C when the metabolic activity is negligible.

To further support this hypothesis, we conducted flow cytometry studies to examine the uptake of fDOX and nDOX by $CD44^+$ *versus* $CD44^-$ mammosphere cells. Figure 4b shows typical flow cytometry peaks demonstrating uptake of fDOX and nDOX by $CD44^+$ (red) *versus* $CD44^-$ (light gray) cell subpopulations in mammospheres after incubating with the drugs at three different time points. There was no clear difference between the two cell subpopulations in terms of fDOX uptake. On the contrary, augmented uptake of nDOX by $CD44^+$ mammosphere cells was noticeable starting at as early as 3 h and the difference increased with longer incubation time. Of note, the seemingly small distances between the two peaks were actually large because of the log scale used. The flow data from three independent runs were further summarized in Figure 4c, which shows that the uptake of fDOX *versus* nDOX by $CD44^+$ cells was significantly different for the three different treatment times ($p = 0.04$, 0.001, and 0.0005 for 3 h, day 3, and day 10, respectively) and the uptake of nDOX by $CD44^+$ *versus* $CD44^-$ cells was

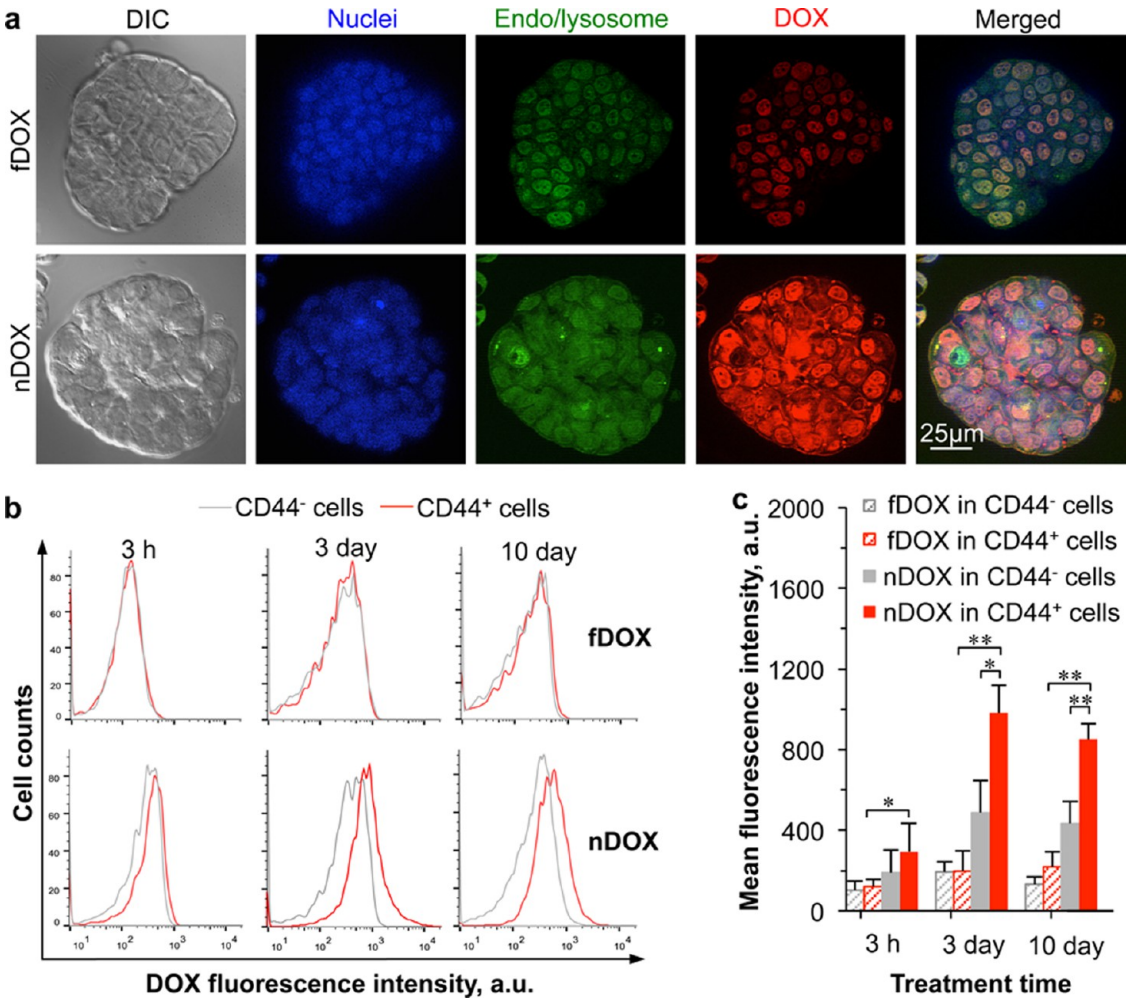

Figure 4. Cellular uptake of nDOX compared to fDOX in mammosphere cells and particularly CD44$^+$ mammosphere cells at 37 °C (with normal endocytic activity). (a) Typical ApoTome SIM (confocal-like) images of cells in a mammosphere after incubating them with 1 μg/mL fDOX or nDOX for 3 h at 37 °C. (b) Typical flow cytometry peaks showing uptake of fDOX and nDOX by CD44$^+$ *versus* CD44$^-$ cells after incubating them with 1 μg/mL fDOX or nDOX for three different times at 37 °C (note: the seemingly small difference in peak intensity is actually large because of the log scale used in the *x* coordinate). (c) Quantitative data of the mean fluorescence intensity of fDOX and nDOX in CD44$^+$ *versus* CD44$^-$ cells. DIC: differential interference contrast. *$p < 0.05$; **$p < 0.01$.

significantly different after 3 (p = 0.015) and 10 (p = 0.005) days incubation. These data explain why the mean fluorescence intensity of DOX in all mammosphere cells (overexpressed with CD44, Figure 1c) and in CD44$^+$CD133$^+$ CSLCs was significantly ($p < 0.01$) much higher for the nDOX than fDOX treatment on days 3 and 10 (Supporting Information Figure S5b,c).

Enhanced Destruction of Mammosphere Cells and CSLCs *in Vitro* by nDOX Compared to fDOX. In view of the enhanced uptake of nDOX in mammosphere cells including CSLCs, we further investigated the cytotoxic effect of nDOX on mammosphere cells including CSLCs in the intact 3D mammospheres (mammosphere 3D model). Suspended single mammosphere cells (dissociated from mammospheres) cultured in the ultralow attachment plate (single cell 3D model) and 2D cultured parent MCF-7 cells (2D model) were also studied for comparison since both models have been conventionally used in the cancer research literature. We tested fDOX *versus* nDOX in destroying the malignant cells in the three different models by incubating them with the cells at various concentrations for up to 10 days. The 10-day treatment time is used to account for possible cancer recurrence on the efficacy of cancer killing *in vitro* by the drugs. Samples with no treatment (NT) or treated with empty nanoparticles (NPs) were also studied in parallel to serve as controls.

Typical images showing morphology of the samples with mammosphere cells under various treatments (drug dose: 1 μg/mL) for 10 days are given in Figure 5a. Many mammospheres were observable in samples with no treatment for both 3D models. The same observation holds true for the samples treated with empty nanoparticles, indicating that the empty nanoparticles are not toxic to the mammosphere cells including CSLCs. Interestingly, both fDOX and nDOX were found to be effective in inhibiting the formation of mammospheres by CSLCs in the single cell 3D model

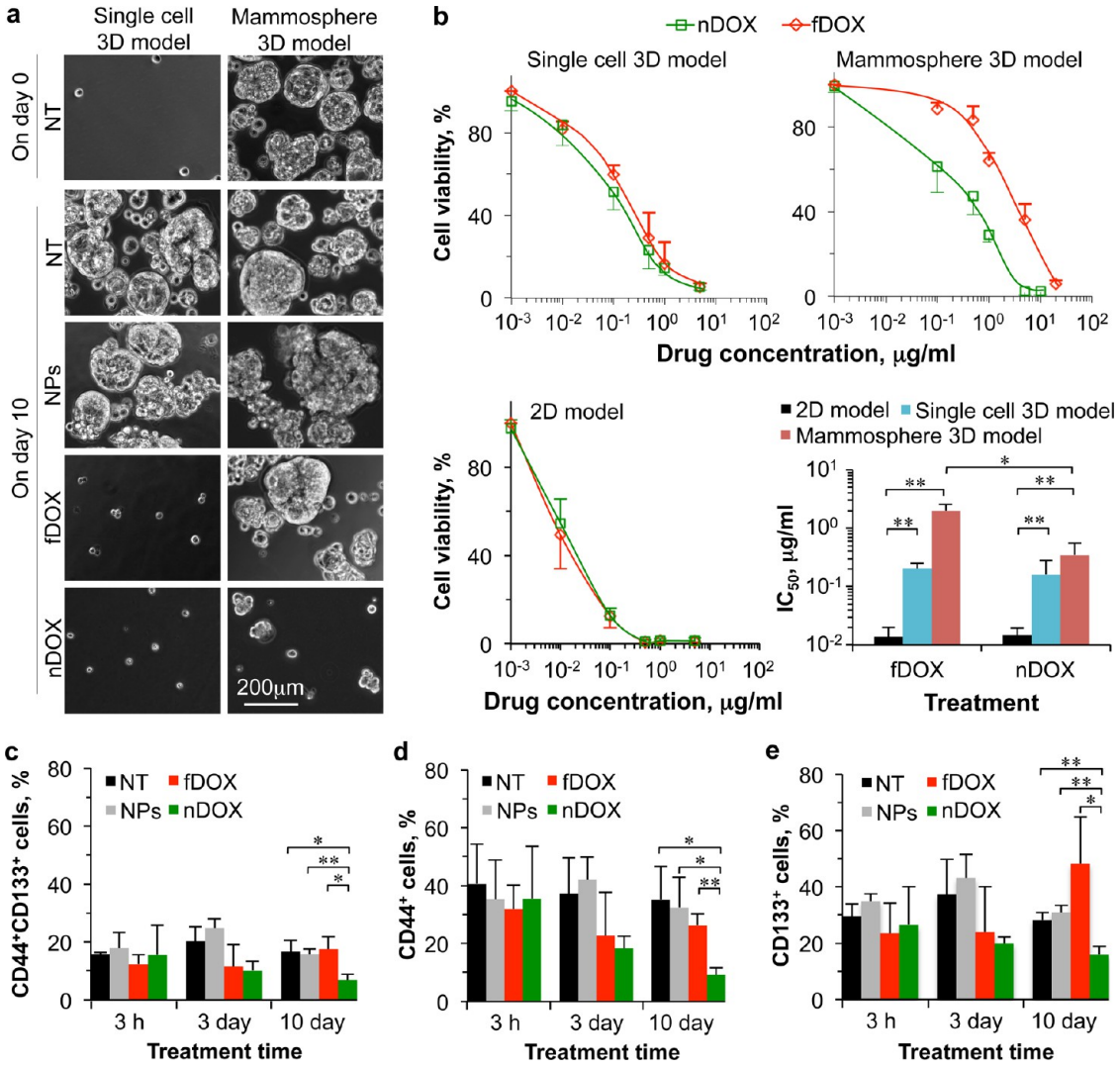

Figure 5. Data of cell viability and percentage of various mammosphere cell subpopulations after various treatments. The results show the mammosphere cells are enriched with CSLCs that reside in intact mammospheres (mammosphere 3D model). They are more resistant to fDOX than dissociated single mammosphere cells in 3D suspension (single cell 3D model) and 2D cultured parent cancer cells (2D model), which can be significantly and greatly reduced by using nDOX. (a) Typical micrographs showing morphology of the cells/mammospheres with various treatments. (b) Survival of mammosphere cells under single cell 3D and mammosphere 3D culture and 2D cultured parent MCF-7 cancer cells after various treatments for 10 days together with a summary of the IC_{50} data for the various conditions. For the mammosphere 3D model, the percentage of (c) $CD44^+CD133^+$, (d) $CD44^+$, and (e) $CD133^+$ cell subpopulations with the various treatments for three different times. NT: no treatment. *$p < 0.05$; **$p < 0.01$.

because no cell aggregate was observable at day 10 in the samples. By contrast, cells including CSLCs in the mammosphere 3D model were more resistant to fDOX with many mammospheres being observable on day 10 in the fDOX treated samples. More importantly, this resistance of the mammosphere cells and CSLCs to fDOX could be effectively overcome by using nDOX in that only few small cell aggregates were observable after 10-day treatment.

The morphological observation was further confirmed quantitatively by the viability of cells in the various samples on day 10. As shown in Supporting Information Figure S6, no significant cytotoxicity (cell viability: ~100%) was observed for empty nanoparticles in the three different *in vitro* cell culture models. The cell survival and the corresponding IC_{50} (inhibitory concentration to reduce cell survival to 50%) data for cells treated with fDOX and nDOX for the three different models are shown in Figure 5b. The IC_{50} for fDOX treatment with the mammosphere 3D model (2.0 μg/mL) was significantly ($p = 0.006$) much higher than that with the single cell 3D model (0.2 μg/mL, 10 times lower) and 2D model (0.01 μg/mL, ~200 times lower), which indicates the markedly enhanced resistance to free anticancer drug of mammosphere cells in the intact 3D mammosphere model compared to the 2D culture parent MCF-7 cells. The IC_{50} for the nDOX treatment of cells in the mammosphere 3D model (0.35 μg/mL) was significantly ($p = 0.01$) and approximately six times lower than that of fDOX (2.0 μg/mL).

The IC_{50} for nDOX treatment with the mammosphere 3D model (0.3 μg/mL) and single cell 3D model (0.2 μg/mL) was both low and not significantly different. For both the 2D model and single cell 3D model, the IC_{50} for nDOX treatment is not significantly different from the fDOX treatment. Taken together, we observed that mammosphere cells including the CSLCs in the intact mammosphere 3D model are much more resistant to free drug (fDOX) than their single cell counterparts in suspension (single cell 3D model) and 2D cultured parent MCF-7 cells, which can be effectively overcome by using the nanodrug (*i.e.*, nDOX) prepared in this study.

We further performed flow cytometry studies to understand how the various treatments (particularly the fDOX and nDOX at 1 μg/mL based on the data shown in Figure 5b to be between the IC_{50}'s of the two drugs for the mammosphere 3D model) could affect the percentage of the $CD44^+CD133^+$, $CD44^+$, and $CD133^+$ cell subpopulations among the mammosphere cells. The results are shown in Figure 5c–e. As expected, treatment with empty nanoparticles (NPs) had no significant impact on the distribution in comparison to the NT (no treatment) control for all the cell subpopulations. Neither fDOX nor nDOX treatment for 3 h appeared to significantly affect the distribution either, presumably because the treatment time was too short for the biological consequences to develop. Although fDOX treatment for 3 days reduced (albeit insignificantly) the average percentage of all the three cell subpopulations compared to NT control, the differences were minimal at day 10 for the $CD44^+CD133^+$ CSLCs and $CD44^+$ subpopulation. The fDOX treatment appeared to even increase (albeit insignificantly) the percentage of $CD133^+$ cell subpopulation in the mammospheres on day 10 (Figure 5e). In other words, the fDOX treatment might show some effectiveness in a shorter time (3 days) but the CSLCs could grow back given a longer time (10 days).

In contrast to fDOX, the nDOX was observed to be potent against the three cell subpopulations in the 3D mammospheres. As shown in Figure 5c, although the nDOX treatment did not change the percentage of CSLCs ($CD44^+CD133^+$) at 3 h compared to NT control, the percentage reduced ($p = 0.067$) on day 3 and the reduction became significant ($p = 0.019$) on day 10. The same trend in percentage and significance held true for nDOX in destroying $CD44^+$ subpopulation ($p = 0.063$ and 0.01 at day 3 and 10, respectively) compared to NT control. For the $CD133^+$ subpopulation, the same trend in reduction of its percentage held true ($p = 0.078$ and 0.0059 at day 3 and 10, respectively) compared to NT control. Compared to fDOX, the nDOX treatment could significantly reduce the percentage of the cell subpopulations ($p = 0.016$, 0.002, 0.017 for $CD44^+CD133^+$, $CD44^+$, and $CD133^+$, respectively). The enhanced cellular uptake of nDOX in $CD44^+CD133^+$ and $CD44^+$ subpopulations of mammosphere cells compared to fDOX (Figure 4 and Supporting Information Figure S5) may explain why nDOX could preferentially destroy the $CD44^+$ subpopulations.

It is worth noting that both the fDOX and nDOX were found to be effective in inhibiting the growth of mammosphere cells including the CSLCs in single cell suspension (single cell 3D model) to form mammospheres. This is possibly because the suspended single CSLCs are in a metabolically and mitotically active (or transit amplifying)[55] state to initiate (or reinitiate) tumor formation. Quiescence/dormancy together with drug efflux by ABC transporters and high resistance to apoptosis has been reported to be the major intrinsic properties that render CSLCs unusually high drug resistance.[16−18] This hypothesis is further supported by the observation that the $CD133^+$ cells in mammospheres are particularly resistant to fDOX treatment (Figure 5e) since CD133 has been suggested to be a marker of quiescent stem cells.[56] It has been reported that various components of the embryonic extracellular matrix components including tenascin and decorin are abundant in mammospheres besides multiple types of cells including the CSLCs.[57] The mammosphere is not a simple assembly of cells, but a microtumor that may contain the CSLC niche including tumor-associated fibroblast, mesenchymal cells, macrophages, and cytokines, and chemokines (paracrines and autocrines) secreted by these various cells so that the CSLCs can be enriched and survive.[19−21] Therefore, the mammospheres should be an excellent microscale 3D tumor model for studying the CSLC drug resistance *in vitro*. Possibly, the 3D niche in mammospheres renders CSLCs in mammospheres more quiescent and drug resistant than CSLCs in single cell suspension.[19−21]

***In Vivo* Tumor-Targeting Capability of nDOX.** To evaluate their tumor targeting capability *in vivo*, biodistribution of the nanoparticles encapsulated with indocyanine green (nICG) was investigated first by intravenous administration of the nICG into orthotopic tumor-bearing mice for noninvasive *in vivo* imaging. Indocyanine green (ICG) was used because it has emission in the near-infrared regime and has been clinically used for noninvasive *in vivo* imaging, while the emission of DOX is in the visible light regime with an optical penetration depth that is too small to image *in vivo* noninvasively. As shown in Figure 6a, strong fluorescence of ICG was observable in tumor at 1 h after intravenous injection and the fluorescence remained in the tumor even at 24 h after injection, suggesting the capability of the chitosan-decorated nanoparticles in targeting tumor *in vivo*. To quantitatively compare the biodistribution of fDOX and nDOX, the amount of DOX was quantified in different organs including heart, brain, liver kidney, spleen, tumor, and blood at 1 h post intravenous injection of the drugs into the orthotopic tumor-bearing mice. As shown in Figure 6b and

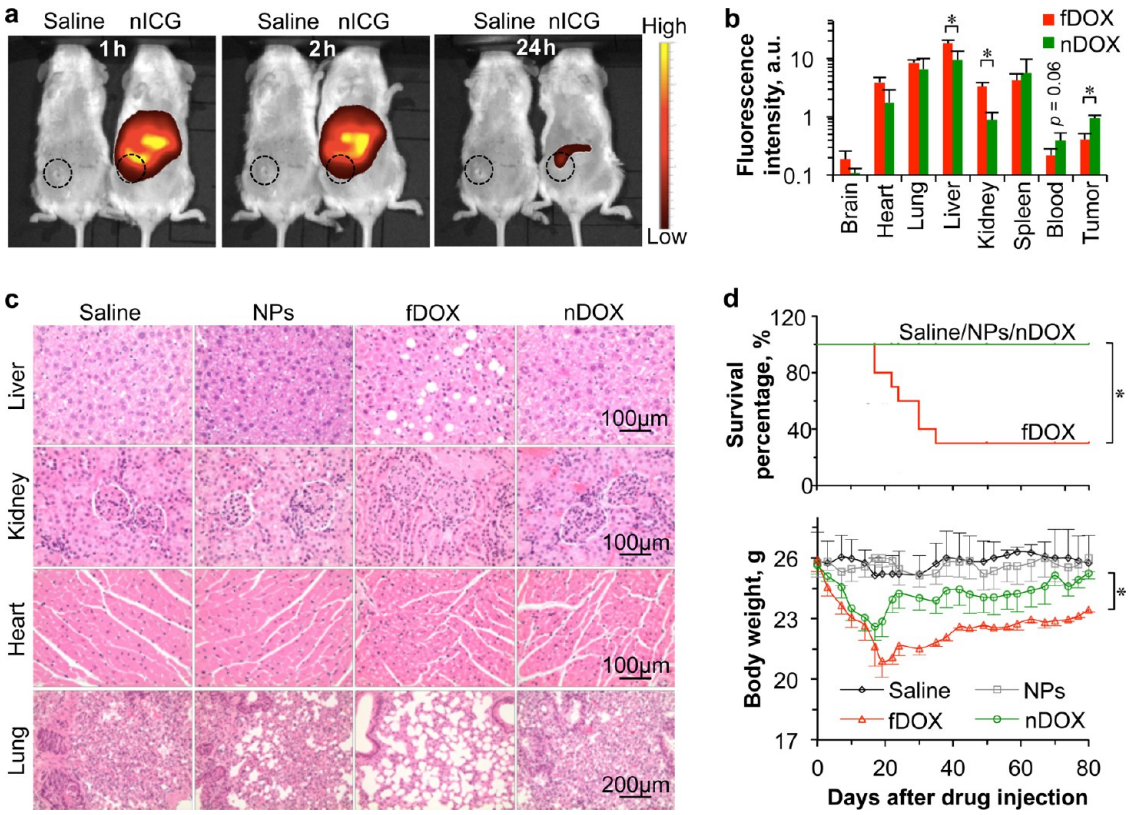

Figure 6. Data on biodistribution, histology, animal survival, and animal body weight showing nDOX is capable of preferentially accumulating in tumor with much reduced systemic toxicity compared to fDOX. (a) Typical images of live imaging showing accumulation of NPs encapsulated with ICG (nICG) in tumor *in vivo* at three different times after intravenous administration of the nICG. (b) Quantitative data of DOX fluorescence intensity in different organs and tumor with fDOX or nDOX treatment. (c) Representative micrographs of hematoxylin and eosin (H&E) staining of four important organs with various treatments. (d) Animal survival after different treatments showing that the treatment with fDOX killed 70% mice, while no mice with treatment of saline, NPs, or nDOX died. The data of animal body weight further shows the much reduced systemic toxicity of nDOX compared to fDOX and negligible toxicity of NPs. *$p < 0.05$.

Supporting Information Figure S7, nDOX rendered a significantly higher (~2.3 time) drug accumulation in tumor than fDOX, further confirming that our nDOX is capable of targeting tumor probably by both passive (EPR effect) and active (chitosan-CD44 interaction) mechanisms (Scheme 1b). On the other hand, compared to fDOX, the use of nDOX significantly reduced the accumulation of drug in liver and kidney and increased (albeit insignificantly, $p = 0.06$) the concentration of drug in blood, which suggests that the use of nDOX could decrease the systemic toxicity of drug to normal tissues/organs while extending the circulation time of the drug in blood to increase its efficacy against cancer.

To further investigate the systemic toxicity and antitumor efficacy of nDOX *versus* fDOX, orthotopic tumor bearing mice treated with the two drugs (twice a week for 2 weeks at 5 mg drug (excluding NPs) per kg body weight) were sacrificed on day 80 after initial drug treatment and various organs/tissues including liver, kidney, heart, lung, and tumor were harvested, fixed, and assessed by histology. The same studies were also conducted for treatments with empty nanoparticles (NPs) to examine their *in vivo* biocompatibility and saline to serve as control. As shown in Figure 6c, fDOX treatment resulted in hepatic damage including macro- and microvesicular steatosis and bile stasis, unlike the other groups. Slight nephrotoxicity was also observable for the fDOX treatment, although it was not severe in any of treatment groups since the fundamental structure of glomeruli was largely preserved. Cellular damage (vacuolization) of cardiac muscle was observed for the fDOX and nDOX treatments, but it is more evident for the fDOX treatment. Severe pulmonary damage with markedly reduced alveolar surface area (honeycomb lung) was seen only for the fDOX treatment.

Likely due to the observed damage in the various organs induced by fDOX, 7 of 10 mice treated with fDOX died within 40 days after the initial drug treatment, while all mice treated with nDOX, NPs, and saline survived even at 80 days after the initial drug treatment (Figure 6d). The high systemic toxicity of fDOX was further supported by the significantly reduced body weight of mice treated with fDOX at day 80, while the body weight of nDOX-treated mice was not

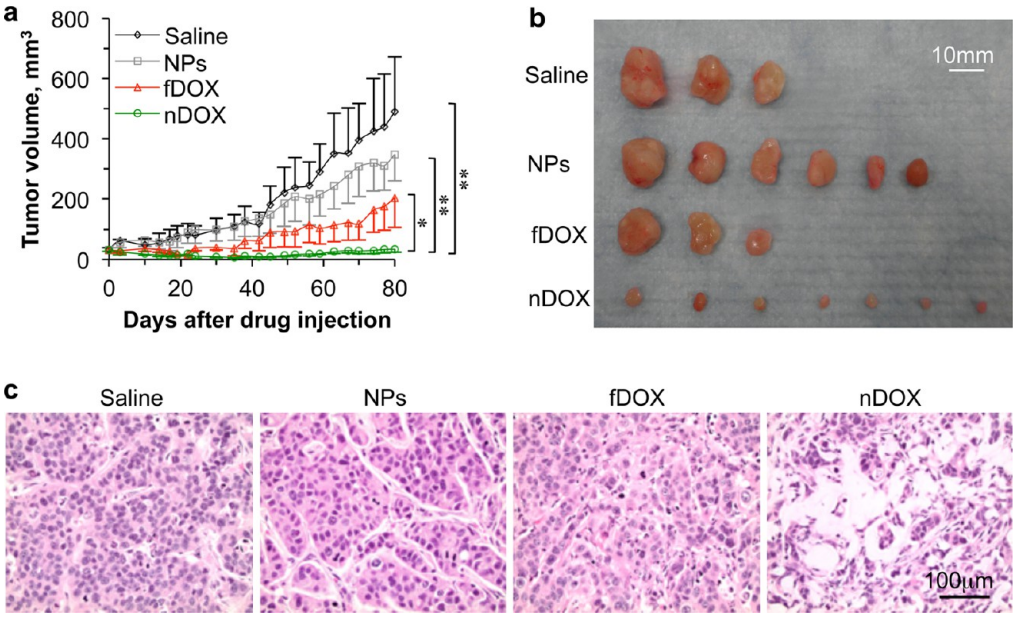

Figure 7. Data of tumor growth and histology showing enhanced anticancer capability of nDOX compared to fDOX. (a) Tumor volume as a function of time for four different treatments. (b) Image of tumors collected on day 80 after initial drug administration for the four different treatments. (c) Representative micrographs of hematoxylin and eosin (H&E) staining of tumors reveal reduced tumoral cellularity with nDOX treatment compared to the other three treatments. *$p < 0.05$; **$p < 0.01$.

significantly different from that of mice in the saline control group, although an apparent drop of body weight was also observed during the initial period of drug administration. The body weight of mice with saline and nanoparticle treatment was not significantly different during the entire period of observation. These data indicate the *in vivo* biocompatibility of our empty nanoparticles and the capacity of significantly reducing the systemic toxicity of fDOX to a tolerable level by using nDOX (*i.e.*, fDOX encapsulated in the nanoparticles).

Enhanced Antitumor Efficacy *in Vivo* of nDOX Compared to fDOX. As shown in Figure 7 and Supporting Information Figure S8, besides the aforementioned *in vivo* biocompatibility, nDOX possesses significantly better antitumor efficacy than fDOX. The treatment with nDOX could significantly better inhibit tumor growth than all the other three treatments (Figure 7a,b and Supporting Information Figure S8). Tumors treated with nDOX were predominately nonviable (necrotic) with decreased tumoral cellularity in viable areas (Figure 7c and Supporting Information Figure S8b). Collectively, these data demonstrate the remarkable antitumor efficacy of nDOX *in vivo*, probably as a result of its enhanced tumor targeting (Figure 6) and killing of $CD44^+$ cancer cells (Figure 5). Our data of the *in vivo* antitumor efficacy at a drug dose of 5 mg/kg body weight (which is equivalent to 5 μg/mL in Figure 5 assuming the tissue density is similar to that of water, 1 g/mL) further support the use of mammosphere 3D *in vitro* model to predict the *in vivo* outcome in comparison to the 2D and single cell 3D *in vitro* models.

CONCLUSION

In this study, we show that mammosphere cells enriched with CSLCs in intact 3D mammospheres or spheroids are significantly more resistant to free doxorubicin hydrochloride (fDOX) than dissociated single mammosphere cells in 3D suspension and 2D-cultured parent (MCF-7) cancer cells. We demonstrated that chitosan could be utilized to decorate nanoparticles and can target CSLCs in spheroids (or mammosphere 3D models) and in tumors in mouse models, *via* its interaction (or binding) with the overexpressed CD44 receptors. Moreover, the binding between the chitosan-decorated nanoparticles and the CD44 receptors overexpressed on normal human adipose-derived stem cells was found to be minimal. These nanoparticles significantly improved drug delivery into tumor while reducing drug accumulation in important normal organs such as the liver and kidney after intravenous injection into the tail vein. As a result, the pH responsive nDOX developed in this study could significantly enhance the capability of the clinically used anticancer drug (DOX) in destroying orthotopic xenograft of human breast cancer in mice with no evident systemic toxicity. While more preclinical studies in murine and large animal models are needed before the nDOX could be translated into the clinic, this work demonstrates the potential of our nanodrug surface-decorated with chitosan to target $CD44^+$ CSLCs, the root of cancer recurrence associated with conventional chemotherapy, for cancer treatment with much improved safety and efficacy. Lastly, it is worth noting that although this study is focused on using DOX for

treating breast cancer, other anticancer drugs could be encapsulated in the chitosan-decorated nanoparticles in the same way and the resultant nanodrug could be used to treat many other types of cancer.

MATERIALS AND METHODS

Materials. Doxorubicin hydrochloride was purchased from Sigma (St. Louis, MO, USA). Pluronic F127 (MW: 12.6 kDa) was obtained from BASF Corp (Wyandotte, MI, USA). Chitosan oligosaccharide of pharmaceutical grade (MW: 1.2 kDa, 95.5% deacetylation) was purchased from Zhejiang Golden-Shell Biochemical Co. Ltd. (Zhejiang, China). The WST-1 cell proliferation reagent was purchased from Roche Diagnostics (Mannheim, Germany). Fetal bovine serum (FBS), penicillin, and streptomycin were purchased from Invitrogen (Carlsbad, CA, USA). The EMEM and DMEM/F-12K cell culture media was purchased from ATCC (Manassas, VA, USA). Hyaluronic acid (HA) was purchased from Lifecore biomedical (Chaska, MN, USA). All other chemicals were purchased from Sigma (St. Louis, MO, USA) unless specifically mentioned otherwise.

Synthesis of Pluronic F127–Chitosan Nanoparticles. The Pluronic F127–chitosan nanoparticles with a core–shell architecture were synthesized using a previously reported method[28] with slight modification. In brief, a total of 500 μL of the 4-nitrophenyl chloroformate (4-NPC) activated (partially, 33.5%)[28] Pluronic F127 (300 mg/mL) in dichloromethane was added dropwise into 5 mL of chitosan solution (15 mg/mL) in deionized (DI) water at pH 10 under sonication using a Branson 450 digital sonifier (Danbury, CT, USA) at 16% of maximum amplitude for 3 min. Dichloromethane was then removed by rotary evaporation. The resultant solution was hydrolyzed by adjusting the solution pH to 12 using sodium hydroxide and then stirred for 30 min to remove any residual 4-NPC that had not reacted with chitosan in the nanoparticles. Afterward, the solution was dialyzed against DI water with a Spectra/Por dialysis tube (MWCO, 50 kDa) overnight and further dialyzed against DI water for 3 h using a 1000 kDa Spectra/Por dialysis tube. Finally, the sample was freeze-dried for 48 h to obtain dry Pluronic F127-chitosan nanoparticles.

Preparation of Nanodoxorubicin (nDOX). To encapsulate hydrophilic free doxorubicin hydrochloride (fDOX, 579.98 Da) in the Pluronic F127–chitosan nanoparticles, 0.2 mg of fDOX and Pluronic F127–chitosan nanoparticles (10 mg) was soaked in 500 μL of DI water at 4 °C when the nanoparticles were swollen with high wall-permeability. After 1 h, the sample was lyophilized at −50 °C for 24 h and further dried at 25 °C for 3 h to remove water both inside and outside the nanoparticles. The dried sample was then put in a humidified oven at 37 °C to shrink the nanoparticles. Then, the shrunken sample was dissolved in 1 mL of warm (37 °C) DI water and the solution was dialyzed against warm DI water with a 20 kDa Spectra/Por dialysis tube for 16 h to obtain clean nDOX by removing non-encapsulated fDOX. The sample was then either used immediately or dried at 37 °C for future use.

Characterization of Pluronic F127–Chitosan Nanoparticles and nDOX. The size and surface zeta potential of the resultant nanomaterials were assessed using a Brookhaven 90 Plus/BI-MAS dynamic light scattering (DLS) instrument by dispersing the nanomaterials (1 mg/mL) in DI water and 1 mM aqueous sodium potassium solution, respectively, according to the manufacturer's instructions. The resultant solutions were then filtered through 0.45 μm filter and the DLS data were obtained after equilibrating the samples at the desired temperatures for at least 30 min.

The morphology of NPs and nDOX was visualized using both scanning (SEM) and transmission (TEM) electron microscopy. For SEM, the dry NPs or nDOX were put on a freshly cleaved mica grid. A thin film of Au was then sputtered onto the NPs or nDOX on the grid. Samples were imaged with an FEI (Hillsboro, OR, USA) NOVA nano400 scanning electron microscope. For TEM imaging, carbon film-coated copper TEM grids were first glow-discharged with a Denton (Moorestown, NJ, USA) DV-502 vacuum evaporator for ~30 s. A total of 1 μL aqueous NPs solution or nDOX solution (4 mg/mL in DI water) was then dropped on the grid and air-dried for ~6–7 min. Afterward, the grid was put in contact with a drop of 12.5 μL of 1% (w/v) uranyl acetate solution on a Ted Pella (Redding, CA, USA) PELCO grid holder pad. Excess solution on the grid was removed by dab drying. Samples were observed with an FEI Tecnai G2 transmission electron microscope. All TEM and SEM experiments were performed at room temperature.

To study the effect of hyaluronidase on the nanoparticle stability, 2.5 mg of nanoparticles was incubated with hyaluronidase (0.2% w/v) in 2.5 mL of DI water at 37 °C for 1 h for further characterization of change in size by DLS at room temperature.

To determine encapsulation efficiency (EE, the weight percentage of DOX encapsulated in nanoparticles out of DOX initially fed for encapsulation) and loading content (LC, the weight percentage of nDOX out of both nDOX and nanoparticles where nDOX is encapsulated), the amount of DOX in various samples was quantified colorimetrically by dispersing it in DI water to measure the absorbance at 480 nm using a Beckman Coulter DU800 UV–vis spectrophotometer. To study release of nDOX from the nanoparticles, a total of 19.8 μg of nDOX dissolved in 1 mL of DI water in a 20 kDa Spectra/Por dialysis tube was dialyzed against 45 mL of DI water at 37 °C with constant stirring. A total of 0.5 mL of the 45 mL dialysate was collected at various times to determine DOX concentration in the dialysate colorimetrically.

Cell Culture. MCF-7 human breast cancer cells (ATCC, Manassas, VA, USA) were cultured in EMEM medium supplemented with 10% FBS, 10 μg/mL insulin, 100 U/mL penicillin, and 100 μg/mL streptomycin at 37 °C in a humidified 5% CO_2 incubator. Medium was changed every other day. Cells between passage 5 and 20 at ~70% confluence were detached for passaging and/or further experimental use. Primary human adipose-derived stem cells (ADSCs) (Lonza, Allendale, NJ, USA) were cultured in ADSC basal medium (Lonza) supplemented with 10% fetal bovine serum (FBS), 5 mL of L-glutamine and 0.5 mL of gentamicin–amphotericin at 37 °C in humidified 5% CO_2 incubator. Medium was changed every other day. Cells at ~80% confluence were detached for passaging and/or further experimental use. Only cells of passage 5 or less were used.

Suspension Culture To Obtain 3D Mammospheres and Spheroids of ADSCs. For mammosphere culture, MCF-7 cells were cultured in 6-well ultralow attachment plates (Corning, Lowell, MA) at a density of 20 000 cells/mL in serum-free DMEM/F12-K supplemented with 5 μg/mL insulin, 20 ng/mL epidermal growth factor, 20 ng/mL basic fibroblast growth factor, 1× B27 (Invitrogen, Carlsbad, CA, USA), 0.4% (w/v) bovine serum albumin, 100 U/mL penicillin, and 100 μg/mL streptomycin. After 10 days culture, the mammospheres were collected for further experimental use. To obtain spheres of ADSCs, single ADSCs were cultured in 6-well ultralow attachment plates at a density of 20 000 cells/mL in ADSC basal medium supplemented with 10% fetal bovine serum (FBS), 5 mL of L-glutamine and 0.5 mL gentamicin–amphotericin. After 2 days culture, the ADSC spheres were collected for further experimental use.

Characterization of Cancer Stem-like Cells (CSLCs). To characterize the expression of cell surface markers, mammospheres were collected by gravity sedimentation, dissociated enzymatically with trypsin/EDTA, and further dissociated by gentle pipetting. Single MCF-7 or dissociated mammosphere cells were washed with 1× PBS and stained with CD44-FITC (Invitrogen, Carlsbad, CA) and CD24-PE (Invitrogen, Carlsbad, CA) antibodies according to the manufacturer's instructions. In addition, single MCF-7 or dissociated mammosphere cells were also stained with CD44-FITC and CD133-APC (Miltenyi Biotec Ltd., Surrey, U.K.) antibodies. Lastly, the stained samples were studied using a BD LSR II Flow Cytometer and the data were analyzed using BD FACSDiva software.

On the basis of CD44 and CD133 staining results, mammosphere cells were further sorted into $CD44^+$ and $CD44^+CD133^+$ subpopulations. Then, the gene expression of MCF-7 cells, mammosphere cells, $CD44^+$ mammosphere cells, and $CD44^+CD133^+$ mammosphere cells was characterized by quantitative RT-PCR (qRT-PCR). The total RNAs from MCF-7 and mammosphere cells were first isolated using RNeasy Mini Kit (Qiagen, Venlo, Limburg, Belgium). Reverse transcription was then carried out using a GeneAmp 9700 PCR system to generate cDNAs with iScript cDNA synthesis kit (BioRad). Finally, qRT-PCR studies were performed with the SYBR Green mix (Bio-Rad, Hercules, CA, USA) using a Bio-Rad CFX96 real time PCR instrument. Relative gene expression was calculated with the $\Delta\Delta C_t$ method[58] using the built-in Bio-Rad software. The genes studied and the corresponding primers used are listed in Supporting Information Table S1. Klf4, Nanog, and Oct4 are pluripotent stem cell genes, cytokeratin (CK) 14 is an early (or basal) epithelial differentiation gene, CK18 is a late (or terminal/luminal) epithelial differentiation gene, and β-2 microglobulin (B2M) was used as the reference (or housekeeping) gene.

Moreover, the expression of three pluripotency protein markers including Oct4, Nanog, and Klf4 was examined using flow cytometry. Briefly, MCF-7 cells, mammosphere cells, $CD44^+$ mammosphere cells, and $CD44^+CD133^+$ mammosphere cells were collected and fixed with 4% paraformaldehyde for 15 min at 4 °C. The fixed samples were blocked with 3% BSA and 0.1% Triton for 1 h and incubated first with primary antibodies for 1 h at room temperature and then secondary antibodies for 1 h at room temperature in dark. Afterward, all the samples were resuspended in 0.2 mL of ice-cold PBS and analyzed using BD LSR-II flow cytometer. The negative controls of these flow cytometry studies were the corresponding cells with no staining. The fluorescence data was analyzed using FlowJo.

***In Vitro* Drug Treatment and Cell Viability.** For drug treatment, 20 000 MCF-7 cells attached in Petri dish (2D model) and mammospheres cells either in single cell suspension (single cell 3D model) or intact in 3D mammospheres (mammosphere 3D model) obtained using the same number of MCF-7 cells were incubated in their respective culture medium containing different concentration of fDOX or nDOX at 37 °C for up to 10 days. As controls, the cells with no treatment (NT) or incubated with nanoparticles (NPs) at the highest concentration (5.1 mg/mL) as that in nDOX were studied in parallel. Morphological survival of cells in the various samples was monitored and imaged using a Zeiss Axio Observer Z1 inverted microscope. The total number of cells in each sample were quantified using WST-1 assay according to the manufacturer's instruction by measuring absorbance at 450 nm using a PerkinElmer VICTOR X4Multilabel plate reader. Cell viability was calculated as the ratio of the cell number determined for each sample to that of control samples with no treatment.

Characterization of Cellular Uptake of DOX. To quantify cellular uptake of fDOX and nDOX using flow cytometry, mammosphere cells were collected at the desired times (3 h, 3 day, or 10 day) of incubation with the drugs, washed with 37 °C 1× PBS, detached using trypsin/EDTA, stained with CD44-FITC and CD133-APC antibodies, and analyzed using a BD LSR-II Flow Cytometer together with BD FACSDiva and FlowJo software. The samples with no treatment or treated with nanoparticles were also studied in the same way in parallel as controls.

Specific Binding between nDOX and CD44 Receptors. To study the specific binding of nDOX to CD44-overexpressing mammosphere cells, the mammospheres were collected and put on ice for 2 h to minimize the metabolic activity. Then, the mammospheres were incubated with 5 μg/mL nDOX for 3 h at 4 °C, washed with 1× PBS, and fixed in 4% paraformaldehyde. The fixed samples were then incubated in 3% BSA in 1× PBST (1× PBS and 0.05% Tween 20) at room temperature for 1 h to block potential nonspecific binding, followed by overnight incubation at 4 °C with primary antibody of CD44 (1:40 dilution, Abcam, Cambridge, MA, USA). The mammospheres were then washed 3 times and incubated in dark at room temperature for 1 h with secondary antibody (goat anti-rabbit IgG tagged with Alexa Fluor 488 from Abcam, Cambridge, U.K.) diluted in 3% BSA in 1× PBST (1:50 dilution). The samples were then washed and further stained for nuclei using Hoechst 33342 (5 μM) for examination using Zeiss (Oberkochen, Germany) ApoTome structured illumination microscopy (SIM) that is confocal-like. Moreover, blocking experiments were also conducted to check whether preincubation of HA with mammosphere cells could reduce the binding of nDOX to the cells. Briefly, the mammospheres were collected and put on ice for 2 h to minimize the metabolic activity. Then, the mammospheres were incubated with excessive HA (1 mg/mL in 1 mL medium) for 0.5 h at 4 °C, washed with 1× PBS, and further incubated with 10 μg/mL fDOX or nDOX. After incubation for 3 h at 4 °C, the samples were washed with PBS and fixed with 4% paraformaldehyde. The fixed samples were further stained for nuclei using Hoechst 33342 (5 μM) for examination using Zeiss ApoTome SIM microscopy. The samples without HA blocking were also studied in parallel.

To study binding between nDOX and CD44 highly expressed on ADSCs, both 2D cultured ADSCs and 3D ADSC spheres were used since they overexpressed CD44 receptors (unlike 2D cultured MCF-7 cells that have minimal expression of CD44). For 2D studies, ADSCs were seeded on type I collagen-coated glass coverslips placed in 6-well plates at a density of 1×10^5 cells per mL medium and incubated overnight for attachment onto the coverslips. Similar aforementioned procedure for studying the binding between nDOX and CD44 receptors on mammospheres was then used for the 2D cultured ADSCs and 3D ADSC spheres. Briefly, the ADSCs were put on ice for 2 h to minimize their metabolic activity. The cells were then incubated with excessive HA (1 mg/mL in 1 mL of ADSCs culture medium) for 0.5 h at 4 °C. Samples without HA blocking were studied in parallel. Afterward, the samples were washed with PBS and incubated with 10 μg/mL fDOX or nDOX. After 3 h incubation at 4 °C, the samples were washed with PBS and fixed with 4% paraformaldehyde. The fixed samples were incubated in 3% BSA in 1× PBST (1× PBS and 0.05% Tween 20) at room temperature for 1 h to block potential nonspecific binding, followed by overnight incubation at 4 °C with primary antibodies of CD44. The samples were then washed 3 times with 1× PBS and incubated in the dark at room temperature for 1 h with secondary antibodies diluted in 3% BSA in 1× PBST (1:50 dilution). The samples were then washed and further stained for nuclei using Hoechst 33342 (5 μM) for further examination using Zeiss ApoTome SIM microscopy.

Animals and Orthotopic Xenografts of Human Mammary Tumor. Immunodeficient NOD/SCID mice were purchased from National Cancer Institute-Frederick Laboratory and were maintained on a 16:8 h light−dark cycle. All procedures for animal use were approved by the Institutional Animal Care and Use Committee (IACUC) at The Ohio State University and all efforts were made to minimize animal suffering. To obtain orthotopic xenograft of human mammary tumor in the mice, detached mammosphere cells were suspended at 5×10^4 cells/mL in a mixture (1:1) of 1× PBS and matrigel. A total of 5000 cells in 100 μL of the mixture were injected into the fat pad of each 6-week-old female NOD/SCID mouse.

***In Vivo* Imaging and Biodistribution.** For *in vivo* imaging studies, after the tumor reached ~5 mm in diameter, the mice were injected with 200 μL of saline or 100 μg of indocyanine green (ICG) encapsulated in the Pluronic F127−chitosan nanoparticles in 200 μL of saline. The procedure for encapsulating ICG in the nanoparticles was the same as that for encapsulation of DOX. *In vivo* fluorescence images were taken at 1, 2, and 24 h after injection using a PerkinElmer (Waltham, MA, USA) IVIS instrument with a 780 nm excitation wavelength and an 831 nm filter to collect the fluorescence signals of ICG. To quantitatively analyze the biodistribution, the mice after injection with nDOX and fDOX (3 mice each group) at 1 h were euthanized and organs including brain, heart, liver, spleen, lung, kidney, and tumor were collected for further analysis. To do this, the organs were homogenized first using a Dounce homogenizer (Fisher scientific, Waltham, MA, USA). Tissue homogenates of 10% (w/v) were then prepared in DI water to further lyse cells. The tissue homogenates or 25% (v/v) blood in a total volume of 200 μL was then transferred into a 2 mL microcentrifuge tube, and 100 μL of 10% (v/v) Triton X-100, 200 μL of DI water, and 1500 μL of

acidified isopropanol (0.75 N HCl) were added. The tubes were mixed thoroughly and the doxorubicin and doxorubicin metabolites (if any) were extracted overnight at −20 °C. On the next day, the tubes were warmed to room temperature, vortexed for 5 min, and centrifuged at 15 000*g* for 20 min; the supernatant of each sample was collected and doxorubicin was quantified fluorometrically with excitation at 490 nm and emission at 585 nm. The data represents the mean ± standard deviation from three mice and are expressed as doxorubicin fluorescence intensity per 0.1 mL of blood or per 0.1 g of tissue.

***In Vivo* Antitumor Efficacy and Systemic Toxicity.** After the tumor reached ∼5 mm in diameter, mice were treated twice a week for 2 weeks with 200 μL of saline ($n = 3$), NPs ($n = 6$), fDOX ($n = 10$, 5 mg/kg body weight), and nDOX ($n = 7$, 5 mg/kg body weight), respectively. NPs, fDOX, and nDOX were dissolved in 200 μL of saline for injection, and the amount of NP used was the same as the nanoparticle content in nDOX. Tumor growth was monitored twice a week. The tumor volume (V) was calculated by the following formula: $V = (L \times W^2)/2$, where L is long diameter and W is short diameter determined using a caliper. The body weight of mice was monitored also twice a week. The mice were euthanized 80 days after the first drug injection. Tumors, livers, lungs, hearts and kidneys were collected, formalin fixed, and paraffin embedded for further histological analysis.

Statistical Analysis. All data are reported as mean ± standard deviation (SD) from at least three independent runs. The statistical significance in mean values between two groups was determined using Microsoft Excel based on Student's two-tailed *t*-test assuming equal variance. For tumor volume study, the statistical significance between the mean values of more than two groups was determined using one-way analysis of variance (ANOVA) and post hoc tests with the Dunnett's multiple comparisons were applied using tumor volumes from saline treatment group as reference. The difference is considered statistically significant when the p value is less than 0.05.

Conflict of Interest: The authors declare no competing financial interest.

Acknowledgment. This work was supported by an American Cancer Society (ACS) Research Scholar Grant (No. 120936-RSG-11-109-01-CDD) to X.H. and a Pelotonia postdoctoral fellowship to H.W. We thank K. Zhang and B. Weekes for their technical help with experiments.

Supporting Information Available: Characterization of stemness of various mammosphere cells based on gene and protein expression; characterization of the nanoparticles using ^{1}H nuclear magnetic resonance; data showing the resemblance of chitosan to hyaluronic acid; data of specific binding showing that nDOX is incapable of binding to the CD44 receptors overexpressed on normal human adipose-derived stem cells (ADSCs); control and quantitative data showing enhanced cellular uptake of nDOX compared to fDOX in all mammospheres and $CD44^+CD133^+$ mammosphere cells; cell viability data showing negligible cytotoxicity of empty nanoparticles; fluorescence spectra showing doxorubicin in various organs; and data of tumor weight and gross histology. The Supporting Information is available free of charge on the ACS Publications website at DOI: 10.1021/nn506928p.

REFERENCES AND NOTES

1. Jordan, C. T.; Guzman, M. L.; Noble, M. Cancer Stem Cells. *N. Engl. J. Med.* **2006**, *355*, 1253–1261.
2. Frank, N. Y.; Schatton, T.; Frank, M. H. The Therapeutic Promise of the Cancer Stem Cell Concept. *J. Clin. Invest.* **2010**, *120*, 41–50.
3. Visvader, J. E.; Lindeman, G. J. Cancer Stem Cells in Solid Tumours: Accumulating Evidence and Unresolved Questions. *Nat. Rev. Cancer* **2008**, *8*, 755–768.
4. Ponta, H.; Sherman, L.; Herrlich, P. A. Cd44: From Adhesion Molecules to Signalling Regulators. *Nat. Rev. Mol. Cell Biol.* **2003**, *4*, 33–45.
5. Louderbough, J. M. V.; Schroeder, J. A. Understanding the Dual Nature of Cd44 in Breast Cancer Progression. *Mol. Cancer Res.* **2011**, *9*, 1573–1586.
6. Zhou, S.; Schuetz, J. D.; Bunting, K. D.; Colapietro, A. M.; Sampath, J.; Morris, J. J.; Lagutina, I.; Grosveld, G. C.; Osawa, M.; Nakauchi, H.; et al. The Abc Transporter Bcrp1/Abcg2 Is Expressed in a Wide Variety of Stem Cells and Is a Molecular Determinant of the Side-Population Phenotype. *Nat. Med.* **2001**, *7*, 1028–1034.
7. Dean, M.; Fojo, T.; Bates, S. Tumour Stem Cells and Drug Resistance. *Nat. Rev. Cancer* **2005**, *5*, 275–284.
8. Hermann, P. C.; Huber, S. L.; Herrler, T.; Aicher, A.; Ellwart, J. W.; Guba, M.; Bruns, C. J.; Heeschen, C. Distinct Populations of Cancer Stem Cells Determine Tumor Growth and Metastatic Activity in Human Pancreatic Cancer. *Cell Stem Cell* **2007**, *1*, 313–323.
9. Al-Hajj, M.; Wicha, M. S.; Benito-Hernandez, A.; Morrison, S. J.; Clarke, M. F. Prospective Identification of Tumorigenic Breast Cancer Cells. *Proc. Natl. Acad. Sci. U.S.A.* **2003**, *100*, 3983–2988.
10. Kruger, J. A.; Kaplan, C. D.; Luo, Y.; Zhou, H.; Markowitz, D.; Xiang, R.; Reisfeld, R. A. Characterization of Stem Cell-like Cancer Cells in Immune-Competent Mice. *Blood* **2006**, *108*, 3906–3912.
11. Bandyopadhyay, A.; Wang, L.; Agyin, J.; Tang, Y.; Lin, S.; Yeh, I. T.; De, K.; Sun, L. Z. Doxorubicin in Combination with a Small Tgfbeta Inhibitor: A Potential Novel Therapy for Metastatic Breast Cancer in Mouse Models. *PLoS One* **2010**, *5*, e10365.
12. Wang, X.; Low, X. C.; Hou, W.; Abdullah, L. N.; Toh, T. B.; Mohd Abdul Rashid, M.; Ho, D.; Chow, E. K. Epirubicin-Adsorbed Nanodiamonds Kill Chemoresistant Hepatic Cancer Stem Cells. *ACS Nano* **2014**, *8*, 12151–12166.
13. Wang, F.; Wang, Y. C.; Dou, S.; Xiong, M. H.; Sun, T. M.; Wang, J. Doxorubicin-Tethered Responsive Gold Nanoparticles Facilitate Intracellular Drug Delivery for Overcoming Multidrug Resistance in Cancer Cells. *ACS Nano* **2011**, *5*, 3679–3692.
14. Gao, Y.; Chen, Y.; Ji, X.; He, X.; Yin, Q.; Zhang, Z.; Shi, J.; Li, Y. Controlled Intracellular Release of Doxorubicin in Multidrug-Resistant Cancer Cells by Tuning the Shell-Pore Sizes of Mesoporous Silica Nanoparticles. *ACS Nano* **2011**, *5*, 9788–98.
15. Kabanov, A. V.; Batrakova, E. V.; Alakhov, V. Y. Pluronic Block Copolymers for Overcoming Drug Resistance in Cancer. *Adv. Drug Delivery Rev.* **2002**, *54*, 759–779.
16. Bapat, S. A. Human Ovarian Cancer Stem Cells. *Reproduction* **2010**, *140*, 33–41.
17. Naumov, G. N.; Bender, E.; Zurakowski, D.; Kang, S. Y.; Sampson, D.; Flynn, E.; Watnick, R. S.; Straume, O.; Akslen, L. A.; Folkman, J.; et al. A Model of Human Tumor Dormancy: An Angiogenic Switch from the Nonangiogenic Phenotype. *J. Natl. Cancer Inst.* **2006**, *98*, 316–325.
18. Chuthapisith, S.; Eremin, J.; El-Sheemey, M.; Eremin, O. Breast Cancer Chemoresistance: Emerging Importance of Cancer Stem Cells. *Surg. Oncol.* **2010**, *19*, 27–32.
19. Marotta, L. L.; Almendro, V.; Marusyk, A.; Shipitsin, M.; Schemme, J.; Walker, S. R.; Bloushtain-Qimron, N.; Kim, J. J.; Choudhury, S. A.; Maruyama, R.; et al. The Jak2/Stat3 Signaling Pathway Is Required for Growth of Cd44(+)Cd24(−) Stem Cell-like Breast Cancer Cells in Human Tumors. *J. Clin. Invest.* **2011**, *121*, 2723–2735.
20. Korkaya, H.; Liu, S.; Wicha, M. S. Breast Cancer Stem Cells, Cytokine Networks, and the Tumor Microenvironment. *J. Clin. Invest.* **2011**, *121*, 3804–3809.
21. Chin, A. R.; Wang, S. E. Cytokines Driving Breast Cancer Stemness. *Mol. Cell. Endocrinol.* **2013**, *382*, 598–602.
22. Du, J.-Z.; Du, X.-J.; Mao, C.-Q.; Wang, J. Tailor-Made Dual pH-Sensitive Polymer−Doxorubicin Nanoparticles for Efficient Anticancer Drug Delivery. *J. Am. Chem. Soc.* **2011**, *133*, 17560–17563.
23. Yao, H. J.; Zhang, Y. G.; Sun, L.; Liu, Y. The Effect of Hyaluronic Acid Functionalized Carbon Nanotubes Loaded with Salinomycin on Gastric Cancer Stem Cells. *Biomaterials* **2014**, 9208–9223.

24. Burke, A. R.; Singh, R. N.; Carroll, D. L.; Wood, J. C. S.; D'Agostino, R. B., Jr; Ajayan, P. M.; Torti, F. M.; Torti, S. V. The Resistance of Breast Cancer Stem Cells to Conventional Hyperthermia and Their Sensitivity to Nanoparticle-Mediated Photothermal Therapy. *Biomaterials* **2012**, *33*, 2961–2970.
25. Wang, C. H.; Chiou, S. H.; Chou, C. P.; Chen, Y. C.; Huang, Y. J.; Peng, C. A. Photothermolysis of Glioblastoma Stem-Like Cells Targeted by Carbon Nanotubes Conjugated with Cd133 Monoclonal Antibody. *Nanomedicine* **2011**, *7*, 69–79.
26. Wang, D.; Huang, J.; Wang, X.; Yu, Y.; Zhang, H.; Chen, Y.; Liu, J.; Sun, Z.; Zou, H.; Sun, D.; et al. The Eradication of Breast Cancer Cells and Stem Cells by 8-Hydroxyquinoline-Loaded Hyaluronan Modified Mesoporous Silica Nanoparticle-Supported Lipid Bilayers Containing Docetaxel. *Biomaterials* **2013**, *34*, 7662–7673.
27. Zhang, W.; Gilstrap, K.; Wu, L.; K, C. R.; Moss, M. A.; Wang, Q.; Lu, X.; He, X. Synthesis and Characterization of Thermally Responsive Pluronic F127-Chitosan Nanocapsules for Controlled Release and Intracellular Delivery of Small Molecules. *ACS Nano* **2010**, *4*, 6747–6759.
28. Rao, W.; Zhang, W.; Poventud-Fuentes, I.; Wang, Y.; Lei, Y.; Agarwal, P.; Weekes, B.; Li, C.; Lu, X.; Yu, J.; et al. Thermally Responsive Nanoparticle-Encapsulated Curcumin and Its Combination with Mild Hyperthermia for Enhanced Cancer Cell Destruction. *Acta Biomater.* **2014**, *10*, 831–842.
29. Riva, R.; Ragelle, H.; des Rieux, A.; Duhem, N.; Jerome, C.; Preat, V. Chitosan and Chitosan Derivatives in Drug Delivery and Tissue Engineering. *Adv. Polym. Sci.* **2011**, *244*, 19–44.
30. Senel, S.; McClure, S. J. Potential Applications of Chitosan in Veterinary Medicine. *Adv. Drug Delivery Rev.* **2004**, *56*, 1467–1480.
31. Ramya, R.; Venkatesan, J.; Kim, S. K.; Sudha, P. N. Biomedical Applications of Chitosan: An Overview. *J. Biomater. Tissue Eng.* **2012**, *2*, 100–111.
32. Bowman, K.; Leong, K. W. Chitosan Nanoparticles for Oral Drug and Gene Delivery. *Int. J. Nanomed.* **2006**, *1*, 117–128.
33. Yomota, C.; Komuro, T.; Kimura, T. Studies on the Degradation of Chitosan Films by Lysozyme and Release of Loaded Chemicals. *Yakugaku Zasshi* **1990**, *110*, 442–448.
34. Kulish, E. I.; Volodina, V. P.; Fatkullina, R. R.; Kolesov, S. V.; Zaikov, G. E. Enzymatic Degradation of Chitosan Films under the Action of Nonspecific Enzymes. *Polym. Sci., Ser. B* **2008**, *50*, 175–176.
35. Cabral, H.; Matsumoto, Y.; Mizuno, K.; Chen, Q.; Murakami, M.; Kimura, M.; Terada, Y.; Kano, M. R.; Miyazono, K.; Uesaka, M.; et al. Accumulation of Sub-100 Nm Polymeric Micelles in Poorly Permeable Tumours Depends on Size. *Nat. Nanotechnol.* **2011**, *6*, 815–823.
36. Farokhzad, O. C.; Langer, R. Impact of Nanotechnology on Drug Delivery. *ACS Nano* **2009**, *3*, 16–20.
37. Fang, J.; Nakamura, H.; Maeda, H. The Epr Effect: Unique Features of Tumor Blood Vessels for Drug Delivery, Factors Involved, and Limitations and Augmentation of the Effect. *Adv. Drug Delivery Rev.* **2011**, *63*, 136–151.
38. Chauhan, V. P.; Stylianopoulos, T.; Martin, J. D.; Popovic, Z.; Chen, O.; Kamoun, W. S.; Bawendi, M. G.; Fukumura, D.; Jain, R. K. Normalization of Tumour Blood Vessels Improves the Delivery of Nanomedicines in a Size-Dependent Manner. *Nat. Nanotechnol.* **2012**, *7*, 383–388.
39. Sykes, E. A.; Chen, J.; Zheng, G.; Chan, W. C. Investigating the Impact of Nanoparticle Size on Active and Passive Tumor Targeting Efficiency. *ACS Nano* **2014**, *8*, 5696–5706.
40. Guttilla, I. K.; Phoenix, K. N.; Hong, X.; Tirnauer, J. S.; Claffey, K. P.; White, B. A. Prolonged Mammosphere Culture of Mcf-7 Cells Induces an Emt and Repression of the Estrogen Receptor by Microrna. *Breast Cancer Res. Treat.* **2012**, *132*, 75–85.
41. Harrison, H.; Simoes, B. M.; Rogerson, L.; Howell, S. J.; Landberg, G.; Clarke, R. B. Oestrogen Increases the Activity of Oestrogen Receptor Negative Breast Cancer Stem Cells through Paracrine Egfr and Notch Signalling. *Breast Cancer Res.* **2013**, *15*, R21.
42. Shipitsin, M.; Campbell, L. L.; Argani, P.; Weremowicz, S.; Bloushtain-Qimron, N.; Yao, J.; Nikolskaya, T.; Serebryiskaya, T.; Beroukhim, R.; Hu, M.; et al. Molecular Definition of Breast Tumor Heterogeneity. *Cancer Cell* **2007**, *11*, 259–273.
43. Lorico, A.; Rappa, G. Phenotypic Heterogeneity of Breast Cancer Stem Cells. *J. Oncol.* **2011**, *2011*, 135039.
44. Wright, M. H.; Calcagno, A. M.; Salcido, C. D.; Carlson, M. D.; Ambudkar, S. V.; Varticovski, L. Brca1 Breast Tumors Contain Distinct $Cd44^{+}/Cd24^{-}$ and $Cd133^{+}$ Cells with Cancer Stem Cell Characteristics. *Breast Cancer Res.* **2008**, *10*, R10.
45. Shackleton, M.; Vaillant, F.; Simpson, K. J.; Stingl, J.; Smyth, G. K.; Asselin-Labat, M. L.; Wu, L.; Lindeman, G. J.; Visvader, J. E. Generation of a Functional Mammary Gland from a Single Stem Cell. *Nature* **2006**, *439*, 84–88.
46. Molyneux, G.; Geyer, F. C.; Magnay, F. A.; McCarthy, A.; Kendrick, H.; Natrajan, R.; Mackay, A.; Grigoriadis, A.; Tutt, A.; Ashworth, A.; et al. Brca1 Basal-Like Breast Cancers Originate from Luminal Epithelial Progenitors and Not from Basal Stem Cells. *Cell Stem Cell* **2010**, *7*, 403–417.
47. Rao, W.; Zhao, S.; Yu, J.; Lu, X.; Zynger, D. L.; He, X. Enhanced Enrichment of Prostate Cancer Stem-Like Cells with Miniaturized 3D Culture in Liquid Core-Hydrogel Shell Microcapsules. *Biomaterials* **2014**, *35*, 7762–7773.
48. Vrignaud, S.; Benoit, J. P.; Saulnier, P. Strategies for the Nanoencapsulation of Hydrophilic Molecules in Polymer-Based Nanoparticles. *Biomaterials* **2011**, *32*, 8593–8604.
49. Weigel, P. H.; Oka, J. A. Temperature Dependence of Endocytosis Mediated by the Asialoglycoprotein Receptor in Isolated Rat Hepatocytes. Evidence for Two Potentially Rate-Limiting Steps. *J. Biol. Chem.* **1981**, *256*, 2615–2617.
50. El-Dakdouki, M. H.; Pure, E.; Huang, X. Development of Drug Loaded Nanoparticles for Tumor Targeting. Part 2: Enhancement of Tumor Penetration through Receptor Mediated Transcytosis in 3D Tumor Models. *Nanoscale* **2013**, *5*, 3904–3911.
51. Mo, R.; Jiang, T.; DiSanto, R.; Tai, W.; Gu, Z. Atp-Triggered Anticancer Drug Delivery. *Nat. Commun.* **2014**, *5*, 3364.
52. Banerji, S.; Wright, A. J.; Noble, M.; Mahoney, D. J.; Campbell, I. D.; Day, A. J.; Jackson, D. G. Structures of the Cd44-Hyaluronan Complex Provide Insight into a Fundamental Carbohydrate-Protein Interaction. *Nat. Struct. Mol. Biol.* **2007**, *14*, 234–239.
53. Naor, D.; Nedvetzki, S.; Golan, I.; Melnik, L.; Faitelson, Y. Cd44 in Cancer. *Crit. Rev. Clin. Lab. Sci.* **2002**, *39*, 527–579.
54. Sleeman, J. P.; Kondo, K.; Moll, J.; Ponta, H.; Herrlich, P. Variant Exons V6 and V7 Together Expand the Repertoire of Glycosaminoglycans Bound by Cd44. *J. Biol. Chem.* **1997**, *272*, 31837–31844.
55. Wang, S.; Garcia, A. J.; Wu, M.; Lawson, D. A.; Witte, O. N.; Wu, H. Pten Deletion Leads to the Expansion of a Prostatic Stem/Progenitor Cell Subpopulation and Tumor Initiation. *Proc. Natl. Acad. Sci. U.S.A.* **2006**, *103*, 1480–1485.
56. Pellacani, D.; Oldridge, E. E.; Collins, A. T.; Maitland, N. J. Prominin-1 (Cd133) Expression in the Prostate and Prostate Cancer: A Marker for Quiescent Stem Cells. *Adv. Exp. Med. Biol.* **2013**, *777*, 167–184.
57. Dontu, G.; Abdallah, W. M.; Foley, J. M.; Jackson, K. W.; Clarke, M. F.; Kawamura, M. J.; Wicha, M. S. In Vitro Propagation and Transcriptional Profiling of Human Mammary Stem/Progenitor Cells. *Gene Dev.* **2003**, *17*, 1253–1270.
58. Zhang, W.; Zhao, S.; Rao, W.; Snyder, J.; Choi, J. K.; Wang, J.; Khan, I. A.; Saleh, N. B.; Mohler, P. J.; Yu, J.; et al. A Novel Core-Shell Microcapsule for Encapsulation and 3D Culture of Embryonic Stem Cells. *J. Mater. Chem. B* **2013**, *1*, 1002–1009.